Ore Geology Reviews 90 (2017) 928–942

Contents lists available at ScienceDirect

Ore Geology Reviews

journal homepage: www.elsevier.com/locate/oregeo

Isotope and fluid inclusion geochemistry of the Cangyuan Pb-Zn-Ag polymetallic deposit in Yunnan, SW China

Xian-Ze Deng [a,b], Yan Tao [a,*], Juan Li [a,b], Feng Xiong [a,b]

[a] State Key Laboratory of Ore Deposit Geochemistry, Institute of Geochemistry, Chinese Academy of Sciences, Guiyang 550081, China
[b] University of Chinese Academy of Sciences, Beijing 100049, China

ARTICLE INFO

Article history:
Received 31 May 2016
Received in revised form 19 May 2017
Accepted 22 May 2017
Available online 9 June 2017

Keywords:
Cangyuan Pb-Zn-Ag deposit
Isotope and fluid inclusion geochemistry
Magmatic-derived fluids
Sanjiang Orogen

ABSTRACT

The Cangyuan Pb-Zn-Ag polymetallic deposit is located in the Baoshan Block, southern Sanjiang Orogen. The orebodies are hosted in low-grade metamorphic rocks and skarn in contact with Cenozoic granitic rocks. Studies on fluid inclusions (FIs) of the deposit indicate that the ore-forming fluids are CO_2-bearing, NaCl-H_2O. The initial fluids evolved from high temperatures (462–498 °C) and high salinities (54.5–58.4 wt% NaCl equiv) during the skarn stage into mesothermal (260–397 °C) and low salinities (1.2–9.5 wt% NaCl equiv) during the sulfide stage. The oxygen and hydrogen isotopic compositions ($\delta^{18}O_{H2O}$: 2.7–8.8‰; δD: −82 to −120‰) suggest that the ore-forming fluids are mixture of magmatic fluids and meteoric water. Sulfur isotopic compositions of the sulfides yield $\delta^{34}S$ values of −2.3 to 3.2‰; lead isotopic compositions of ore sulfides are similar to those of granitic rocks, indicating that the sulfur and ore-metals are derived from the granitic magma. We propose that the Cangyuan Pb-Zn-Ag deposit formed from magmatic hydrothermal fluids. These Cenozoic deposits situated in the west of Lanping-Changdu Basin share many similarities with the Cangyuan in isotopic compositions, including the Laochang, Lanuoma and Jinman deposits. This reveals that the Cenozoic granites could have contributed to Pb-Zn-Cu mineralization in the Sanjiang region despite the abundance of Cenozoic Pb-Zn deposits in the region, such as the Jingding Pb-Zn deposit, that is thought to be of basin brine origin.

© 2017 Elsevier B.V. All rights reserved.

1. Introduction

The Cangyuan Pb-Zn-Ag polymetallic deposit is located in the southern part of the Sanjiang metallogenic belt (Hou et al., 2007; Deng et al., 2014). The Sanjiang region exhibits intensive Cenozoic magmatism owing to Indo-Asian collision and reserves numerous deposits, including the granite-related Sn deposits in the Tengchong Block, the Pb-Zn-Cu-Ag polymetallic deposits in the central micro-blocks, and the porphyry Cu-Au-Mo deposits along the Jinshajiang suture (Liu et al., 1993; Xu and Mo, 2000; Xu et al., 2008; Zhou et al., 2012) (Fig. 1). The Pb-Zn-Cu-Ag polymetallic deposits in the central micro-blocks constitute a giant base-metal mineralization belt that contains many large or giant Pb-Zn deposits, such as the Jinding Zn-Pb deposit in the Lanping Basin (Xue et al., 2002a,b), the Zhaofayong Zn-Pb deposit in the Changdu Basin (Tang et al., 2006), the Dongmozhazhua Zn-Pb deposit in the Yushu Basin and the Chaqupacha in the Tuotuohe region (Song et al., 2013).

Studies of Zn-Pb deposits in Lanping Basin have suggested that the Cenozoic Zn-Pb deposits in central micro-blocks of the Sanjiang region are similar to Mississippi Valley Type (MVT) and have no relationship with the magma (Hou et al., 2007; Song et al., 2013). Recent studies indicate that the ore deposits in the Lanping–Simao Basin may be diverse in origin, part of them are basin-brine origin whereas others are magmatic hydrothermal origin, or even linked with fluids from the mantle (Zhao, 1989; Wang and Li, 1991; Zhou and Zhou, 1992; Zhang, 1993; Xue et al., 2000, 2002a,b, 2003). The Cangyuan Pb-Zn-Ag polymetallic deposit has close spatial relationship with Cenozoic granites and provides a good example for investigating the relationship between mineralization and magmatism. Therefore, it would be helpful to understand the metallogenic system of the Sanjiang region.

There are a few studies conducted on the Cangyuan deposit (Xiao et al., 2008). However, the relationship between granites and mineralization is unclear, and the geochemistry and origin of the deposit have not been well constrained. In this study, we conduct detailed analysis on fluid inclusions (FIs) and H-O-S-Pb isotopes of the deposit. Our main objectives are to identify the

* Corresponding author at: State Key Laboratory of Ore Deposit Geochemistry, Institute of Geochemistry, Chinese Academy of Sciences, 99 West Lincheng Road, Guiyang 550081, China.
E-mail address: taoyan@vip.gyig.ac.cn (Y. Tao).

http://dx.doi.org/10.1016/j.oregeorev.2017.05.034
0169-1368/© 2017 Elsevier B.V. All rights reserved.

sources of metals and ore-forming fluids, revealing the formation processes of the deposit, and devote to shed a new light on metallogenic system of the Sanjiang region.

2. Geological background

During the Cenozoic, accompanied with the subduction of Indian Plate, India-Asia collision and breakoff of oceanic slab, numerous Cenozoic magmatic rocks formed in the Sanjiang region (Fig. 1; Deng et al., 2014; Dupont-Nivet et al., 2010; Tao et al., 2009; Williams et al., 2001). The Tengchong and Cangyuan comprise S- and I-type granites with ages of 62–40 Ma (Xu et al., 2012; Chen et al., 2014, 2008, 2010). The granitic rocks in the Tengchong Block are explained as products of Neo-Tethys ocean subduction (Xu et al., 2012), whereas the Cangyuan granites are thought to be formed by crust-mantle mixing (Chen et al., 2008). These granitic rocks share a good relationship with mineralizations of Sn, Pb, Zn, Ag and Cu. An Eocene-Oligocene potassic-ultrapotassic magmatic belt occurs in the vicinity of, as well as distal to, the Jinshajiang-Ailaoshan tectonic belt, extending for thousands of kilometers (Chung et al., 1998). The intrusive felsic rocks yield zircon U-Pb ages of 41, 36 and 35 Ma (Rui et al., 1984; Tang and Luo, 1995; Hou et al., 2003; Guo et al., 2006; Jiang et al., 2006; Liang et al., 2006; Lu et al., 2012).

Although few intrusive rocks occur in the Lanping-Simao Basin, Oligocene MVT Pb-Zn polymetallic deposits are widely distributed with giant metal reserves (Xue et al., 2007).

The studied deposit is distributed in the Cangyuan domain, Baoshan Block. The Baoshan Block is separated from the Tengchong Block in the west by the Gaoligongshan Fault and from Lanping-Simao Basin by the Changning-Menglian suture in the east (Fig. 1). It consists of a late Neoproterozoic to middle Cambrian basement and is covered by Cambrian to Mesozoic sedimentary, which are composed of shallow marine carbonates and clastic rocks.

During the Neotethys movement, the Baoshan Block is affected by subduction of the Neotethyan oceanic plate, removal of the lower lithospheric mantle and underthrusting of the South China plate (Deng et al., 2014). The tectonic-thermal event caused magmatism and related skarn deposits in the Baoshan Block (e.g., Hetaoping and Cangyuan Zn-Pb deposits), which yield ages of 116 Ma and 40 Ma, respectively (Tao et al., 2010; Yang, 2010).

3. Deposit geology

3.1. Deposits

The Cangyuan Pb-Zn-Ag polymetallic deposit is located in the southwestern part of the Baoshan Block, including five ore blocks at Majiadi, Huguangzhai, Gonlang, Jinla, and Mangha (Fig. 2). It is hosted in skarn and a suit of Precambrian low grade metamorphic rocks including the Wangya and Yungou formations. The Wangya Formation consists of schist, phyllite, marble, and metamorphosed volcanic rocks while the Yungou Formation consists of marble, schist and phyllite.

The deposit is controlled by NE-trending thrusts and NW-trending faults (Xiao et al., 2008; Yang, 2010). The NE-trending thrusts, developed along the axial plane of the Zhenkang anticline, were caused by collision of the Indian Plate and the Sanjiang terrane in the Cenozoic; the EW-trending faults formed subsequently.

Cenozoic igneous intrusions are exposed along the NE-trending faults, including K-feldspar granites, granodiorite and granite porphyry. The granitic rocks formed from 41 to 40 Ma (Yang, 2010). The K-feldspar granites are distributed in the southwestern of the deposit and extend to Burma. The intrusions in the Jinla and Mangha ore blocks are granite porphyry (Fig. 4A), whereas in the Huguangzhai block is granodiorite. The granite porphyry contains phenocrysts of potash feldspar, plagioclase, quartz and minor biotite, while the granodiorite contains more plagioclase than potash feldspar. All granitic rocks contain similar accessory minerals such as zircon and apatite.

The alteration within the deposit consists of skarn and sulfide alteration; the skarn occurs in the contact between the granite porphyry and limestone, whereas sulfide alteration is generally located within distal metamorphic rocks. The skarn alteration is zoned from the granite porphyry outwards to the distal limestone, with potassic alteration occurring within the granite porphyry adjacent to the skarn. The proximal skarn consists of garnet-diopside adjacent to the potassic-altered granite porphyry; this assemblage is dominated by garnet with minor amounts of diopside. The garnet-diopside zone is followed by a garnet-diopside-chlorite skarn zone that contains chlorite (Fig. 4C).

3.2. Orebodies

The Jinla ore block consists of three orebodies: V1, V2 and V3 (Fig. 2). The V1 orebody occurs along the NW-trending thrust and is hosted in the skarn zone between granite porphyry and limestone. It strikes for 350 m, with width of 87.1 m and average thickness of 4.72 m. The V2 orebody occurs in the sulfide alteration zone, with mean thickness of 4.71 m and is controlled by the NE-trending thrust. The V3 orebody is controlled by NW-trending fractures in low grade metamorphosed rocks (Fig. 3) and has a thickness of 2–15.5 m. The orebody at Mangha is hosted in the hanging-wall phyllite, whereas the granite porphyry occurs in the footwall and strikes along the NW-trending fracture. The orebodies at Gonlang, Huguangzhai and Majiadi are hosted in the marble and controlled by the NE-trending thrust. Most orebodies are rich with a total Zn + Pb grade of 15 wt% (Yang, 2010).

3.3. Mineral assemblages and mineralization stages

In the Jinla ore block, the main ore minerals are galena, sphalerite, pyrite, and chalcopyrite. The major gangue minerals include garnet, diopside, chloride, quartz and calcite. The sulfide ores occur as disseminated or massive in early quartz-sulfide veins with minor in calcite-sulfide veins (Fig. 4D, E). The sulfide veins cut altered granite porphyry or skarn (Fig. 4B, D) in the V1 orebody. In the V2/3 orebodies, sulfide veins infill fractures in the wall rocks. Pyrite and quartz are cut by sphalerite and chalcopyrite, or replaced by galena (Fig. 4F, G).

In the Mangha ore block, the main ore minerals are galena, sphalerite, pyrite, chalcopyrite, arsenopyrite and pyrrhotite; major gangue minerals are quartz and calcite. The sulfide ores occur mainly as calcite-sulfide vein and infill former fractures in metamorphic rock (Fig. 4H, I). The quartz-sulfide veins (pyrrhotite + sphalerite + cryptocrystalline pyrite) are cut by late calcite-sulfide veins (sphalerite + chalcopyrite + fine-grained pyrite + galena; Fig. 4H, I, K, L). Three types of pyrite occur in the deposit: colloidal pyrite, cryptocrystalline pyrite and fine-grained pyrite (Fig. 4J, L). The colloidal pyrite formed in the sedimentary stage and is replaced by pyrrhotite, arsenopyrite and cryptocrystalline pyrite (Fig. 4J). The fine-grained pyrite formed in late calcite-sulfide veins (Fig. 4L).

Considering the mineralogical assemblages and crosscutting relationships, the Cangyuan Pb-Zn-Ag deposit can be divided into skarn stage and sulfide stage (Fig. 5). The skarn stage consists of garnet, diopside and chlorite. The sulfide stage contains most sulfide ores and can be subdivided into quartz-sulfide stage and calcite-sulfide stage. The quartz-sulfide stage is the main mineralization stage for the Jinla ore block while the calcite-

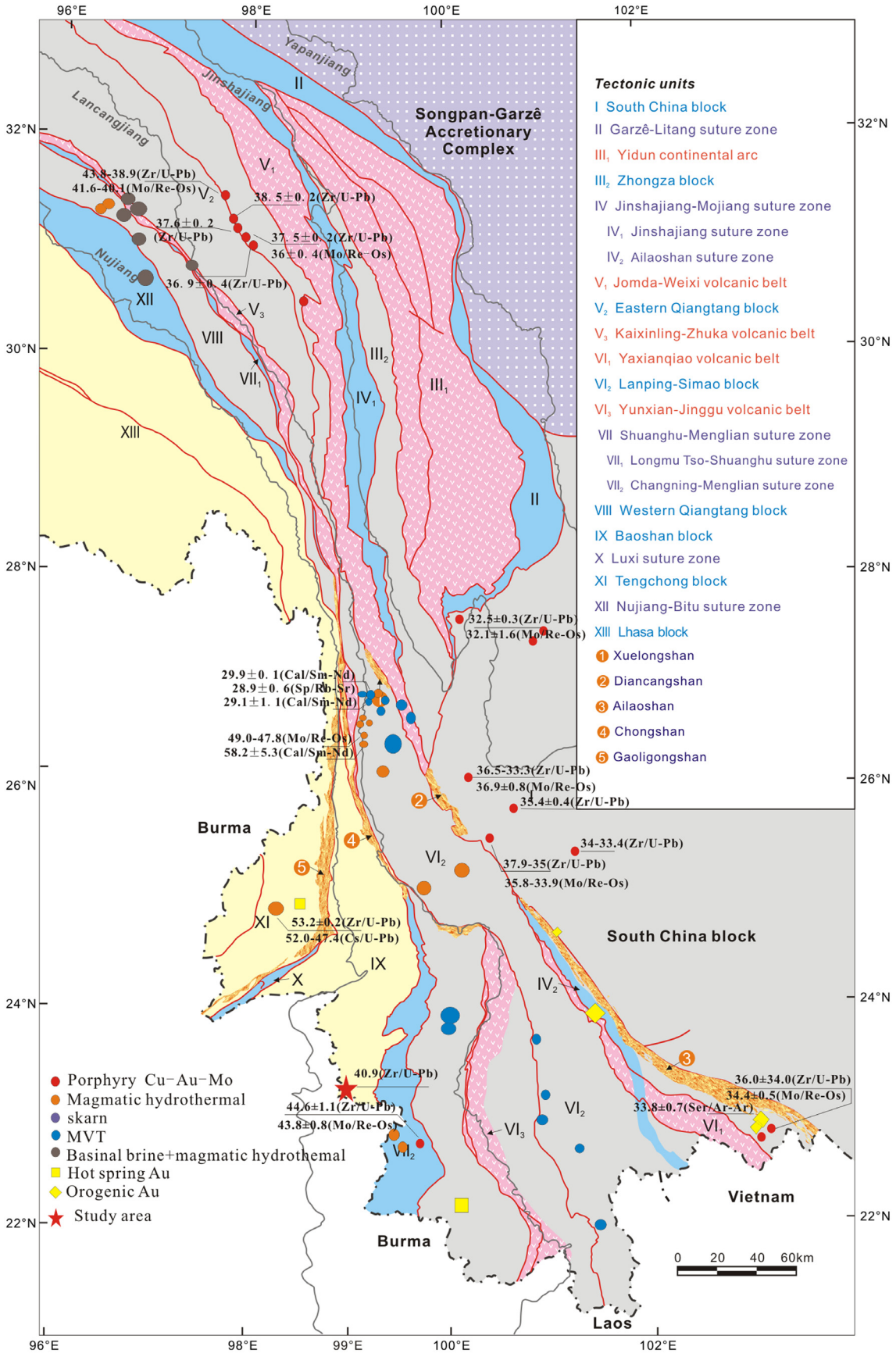

Fig. 1. Distribution of Cenozoic ore deposits in Sanjiang, adapted from Deng et al. (2013).

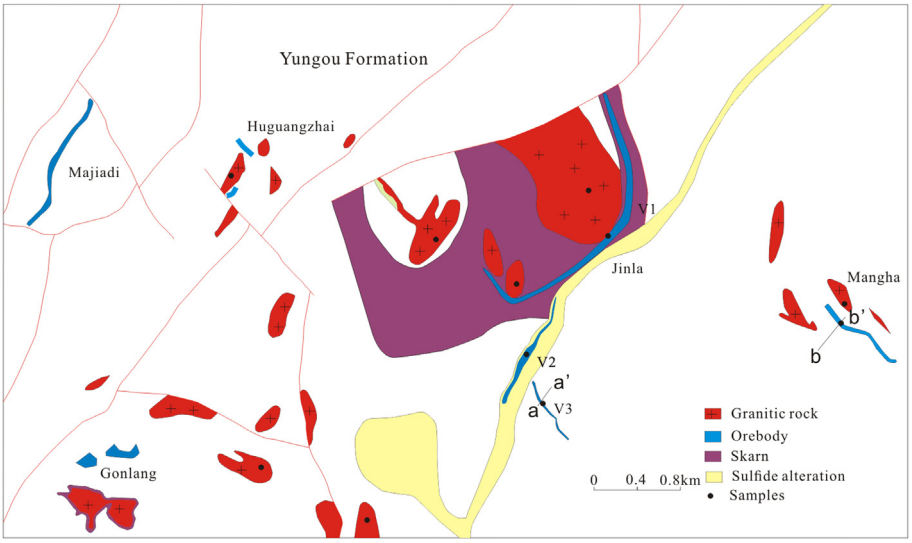

Fig. 2. Geological map of the Cangyuan deposit.

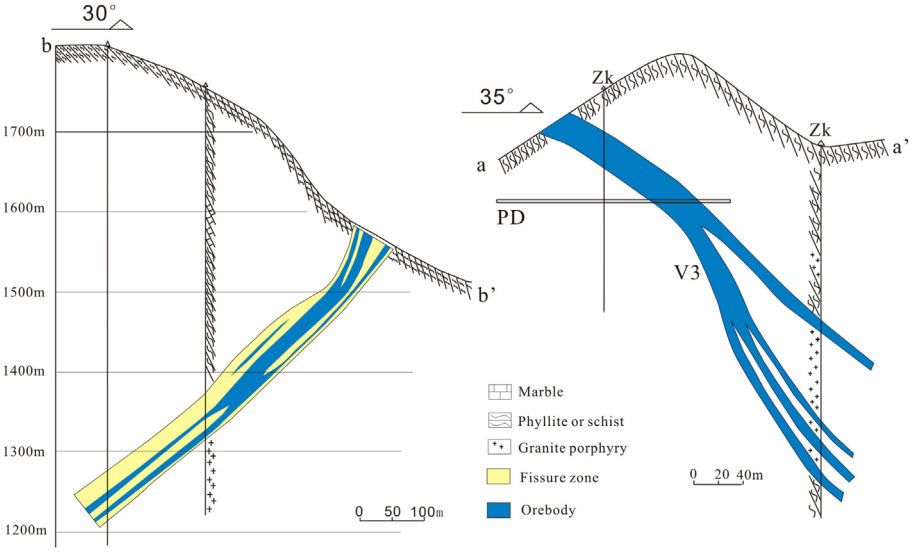

Fig. 3. Cross sections of the Mangha orebody (left) and the Jinla V3 orebody (right).

sulfide stage is the main mineralization stage for the Mangha ore block.

4. Samples and analytical methods

The sulfide ore samples were taken from the Mangha and Jinla ore blocks; the granitic rocks are unaltered. The locations of the samples are shown in Fig 2.

Microthermometric measurements were conducted at the Fluid Inclusion (FI) Laboratory of the Institute of Geochemistry, Chinese Academy of Science, by using the Linkam THMSG600 heating-freezing stage and standard procedures. Stage calibration was performed at −56.6 °C, −10.7 °C and 0.0 °C using synthetic fluid inclusions supplied by FLUID INC with temperatures ranging from −196 °C to 600 °C. The melting temperatures of solid CO_2 ($T_{m,\ CO2}$), freezing point of NaCl-H_2O inclusions ($T_{m,\ ice}$), final melting temperatures of the clathrate ($T_{m,\ cla}$), homogenization temperatures of vapor CO_2 + liquid CO_2($T_{h,\ CO2}$) and total homogenization temperatures of FIs (T_h) were measured at a precision of ±0.1 °C for <10 °C,±1 °C for the interval of 10-300 °C, and ± 2 °C for >300 °C. The heating rate was 10–15 °C/min during the first stages of each heating run, then 2–5 °C/min followed by 0.5−1 °C/min at the phase change points. The salinities of carbonic (CO_2-H_2O), two-phase (vapor + liquid) and three-phase (vapor + liquid + solid) inclusions were calculated by using the final melting temperatures of CO_2-clathrate (Collins, 1979), ice points (Bodnar, 1993) and halite melting temperatures (Hall et al., 1988), respectively. The trapping pressure of the inclusions was estimated on the basis of the CO_2-H_2O-NaCl and H_2O-NaCl system by using the Flincor program (Brown, 1989), the formula of Brown and Lamb (1989), and a pressure (P)-temperature (T) diagram (Bodnar and Vityk, 1994).

The compositions of the individual fluid Inclusions were obtained by using In Via Reflex Laser Raman spectroscopy produced by Renishaw company at the State Key Laboratory of Ore Deposit Geochemistry, Chinese Academy of Science. An argon laser

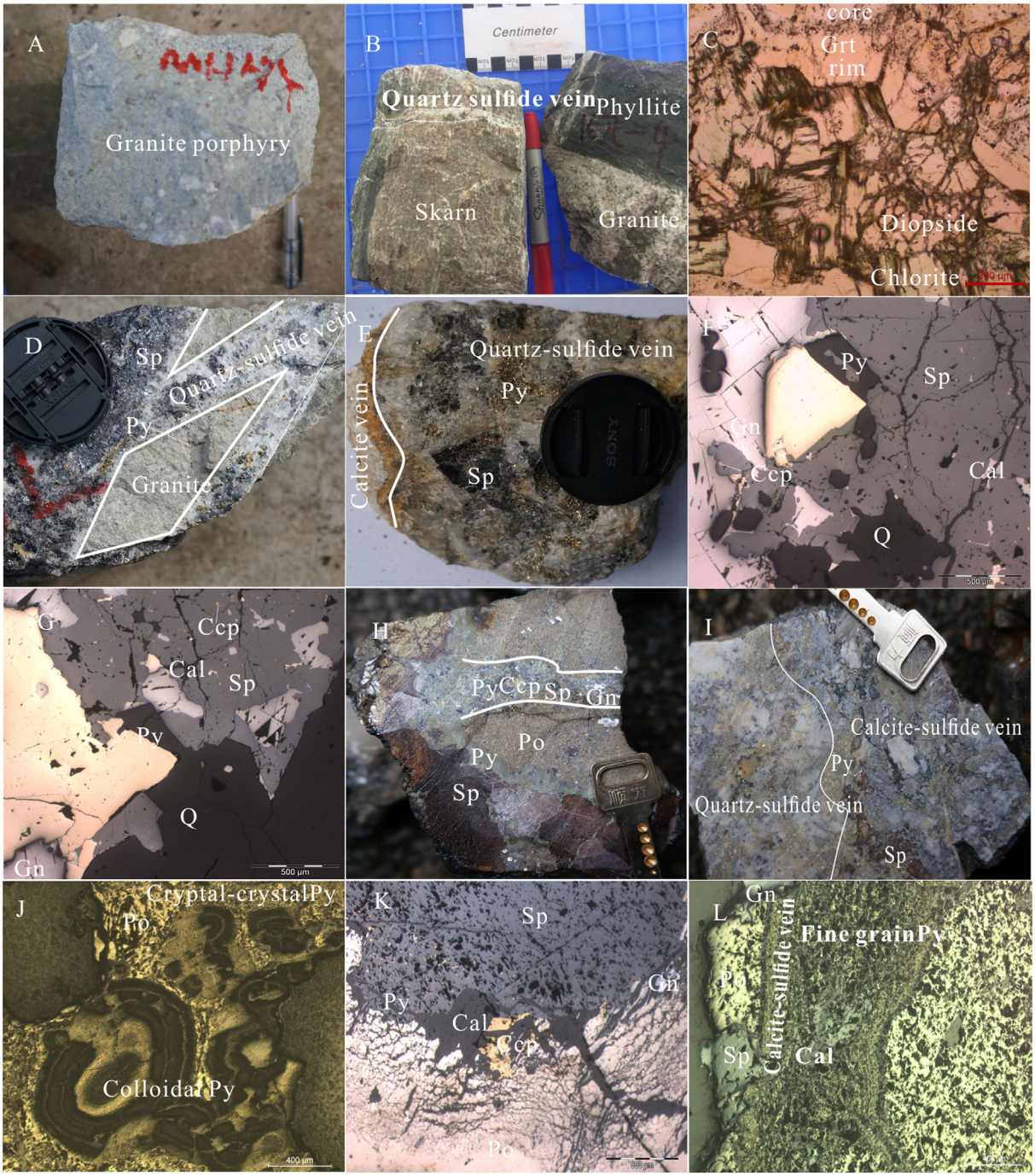

Fig. 4. (A) Granite porphyry in the deposit; (B) Quartz-sulfide vein crosscutting skarn (left) and granite fracturing phyllite (right) at the Jinla ore block; (C) Garnet, diopside and chloride in Skarn from the Jinla ore block; (D) Quartz-sulfide vein fracturing and infilling original limestone and altered granite porphyry at the Jinla ore block; (E) Calcite–sulfide vein crosscutting quartz–sulfide vein at the Jinla ore block; (F/G) Sphalerite + chalcopyrite crosscutting automorphic pyrite and quartz, and a galena and calcite vein crosscutting sphalerite + chalcopyrite at the Jinla block; (H) Co-existing sphalerite + chalcopyrite + galena vein cutting former crypto-crystal pyrite, pyrrhotite and sphalerite (Mangha ore block); (I) Poor quartz-sulfide vein and late rich calcite-sulfide vein (Mangha ore block); (J) Pyrrhotite and crypto-crystal pyrite replacing colloidal pyrite; (K/L) Late sphalerite + galena + calcite cutting former pyrrhotite + pyrite + chalcopyrite. Qz, quartz; Py, pyrite; Gn, galena; Sp, sphalerite; Ccy, chalcopyrite; Po, pyrrhotite; Cal, calcite; Grt, garnet.

with a wavelength of 514 nm was used as the laser source at power of 20 mW power; the spectral range for the analysis was 200–4000 cm^{-1}; the integration time was 60 s and 180 s for some identical inclusions; and the beam size is 1–2 μm.

The minerals used for isotope analyses were selected from the specimens by microscopy. Quartz and sulfides aggregates were separated from the specimens by crushing into grains with size of 40–60 mesh. After panning and filtration, more than 5 g of clear quartz was picked out for each sample under a binocular microscope. To eliminate other interlocking minerals (e.g., sulfides), the quartz grains were soaked in an HNO_3 solution at 60–80 °C for 12 h and were then washed by deionized water. The quartz was dried in an oven at 120 °C prior to analysis. For sulfides, approximately 50 mg was first handled with ace-tone to remove surface contamination and was then washed by deionized water and dried at 60 °C in an oven.

The hydrogen and oxygen isotope ratios of the quartz were analyzed at the Institute of Geology and Geophysics, Chinese Academy

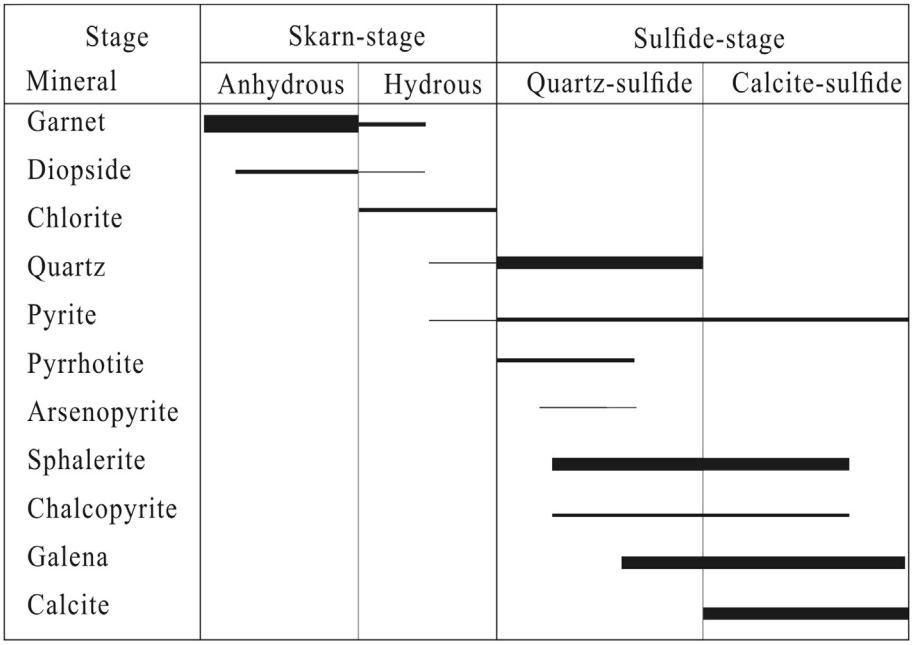

Fig. 5. Mineral paragenesis of the Cangyuan deposit.

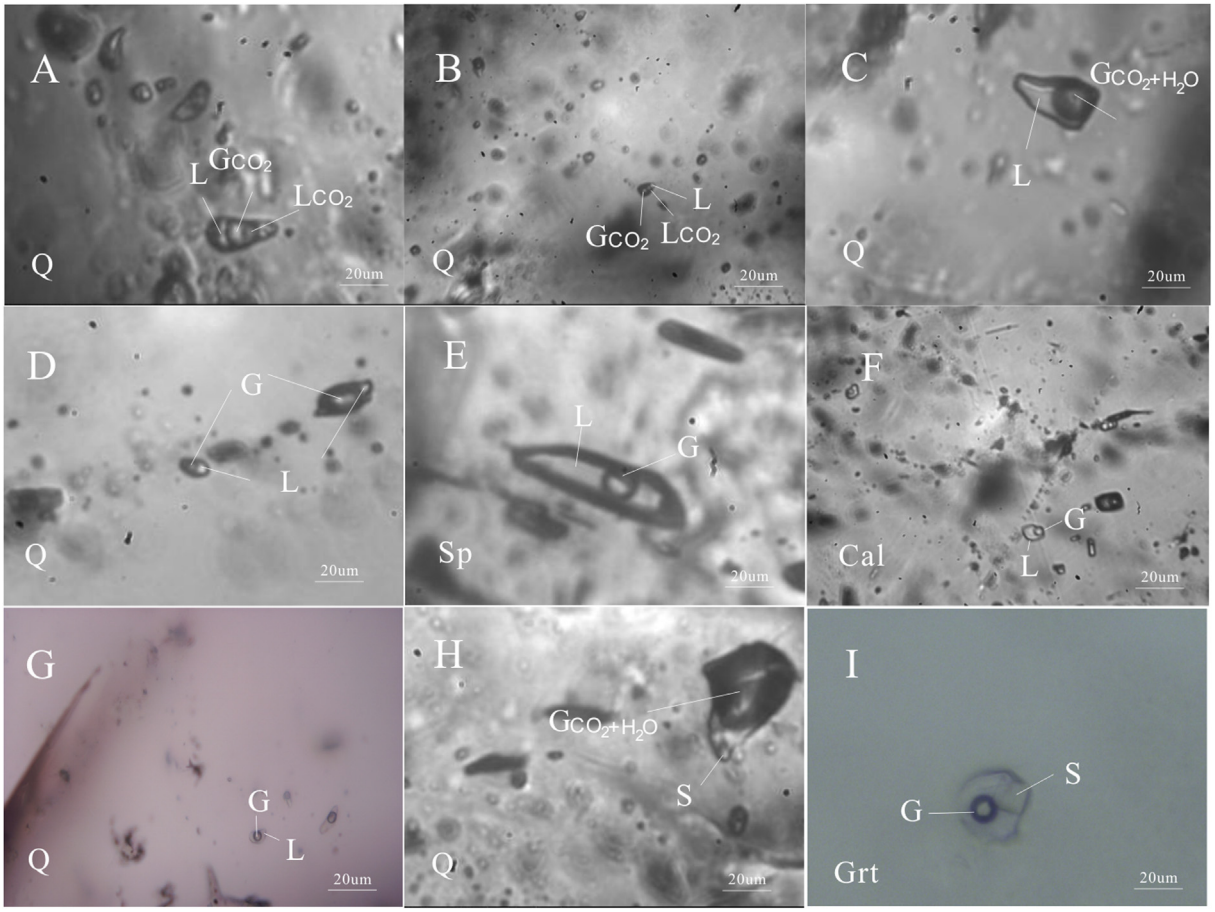

Fig. 6. Photomicrographs of fluid inclusions in quartz, sphalerite and calcite from the Cangyuan deposit. (A) C-type FI ($L + G_{CO2} + L_{CO2}$) in quartz at the Jinla block; (B) C-type FI ($L + G_{CO2} + L_{CO2}$) in quartz at the Mangha block; (C) W1-type FI ($L + G_{CO2+H2O}$) in quartz at the Jinla block; (D) Boiling FIs in quartz at the Jinla block; (E) W2-type FI ($L + G_{H2O}$) in sphalerite at the Mangha block; (F) W2-type FI ($L + G_{H2O}$) in calcite at the Mangha block; (G) W2-type FI ($L + G_{H2O}$) in quartz at the Jinla block; (H) S1-type FI ($L + G_{CO2+H2O} + S$) in quartz at the Jinla block, dauter mineral is calcite; (I). S2-type FI ($L + G_{H2O} + S$) in garnet of skarn at the Jinla block, daughter mineral is halite. Abbreviation: Q, quartz; Sp, sphalerite; Cal, calcite; Grt, garnet.

of Sciences. Samples were put into a quartz tube and were heated to 100 °C for 30 min to eliminate secondary inclusions. Next, they were heated to 600 °C until the fluid inclusions broken. Hydrogen was analyzed by using a MAT253 with 2.0‰ precision, and oxygen was analyzed by using a MAT252 with 0.2‰ precision.

The sulfur isotope ratios of sulfides were analyzed on SO_2 by using Delta–S mass spectrometer at the State Key Laboratory of Environment Geochemistry, Chinese Academy of Sciences. The S-isotopic compositions were reported relative to the Canyon Diablo Triolite (CDT) standard. GBW 04415 and GBW 04414 Ag_2S were used as external standards. The relative errors (2σ) were better than 0.1‰ from the analyses of standard materials.

Sulfide and K-feldspar were analyzed for Pb isotopes by using Laser Ablation Inductively Coupled Plasma Mass Spectrometry (LA-ICP-MS) on a polished section and a rock slide, respectively, at the State Key Laboratory of Continental Dynamics, Northwest University in Xi'an, China. Lead isotope analyses were conducted by using an LA microprobe attached to a Nu Plasma Information Management Corporation ICP-MS system with a beam diameter and width of 30um and 120um, respectively. The typical ablation time was 30 s, and collection times were 50 s. Helium carrier gas transported the ablated aliquot from the laser-ablation cell via a mixing chamber to the ICP-MS torch. Analytical results for the standard NIST610 are $^{208}Pb/^{204}Pb = 36.980 \pm 0.006$ (σ), $^{207}Pb/^{204}Pb = 15.515 \pm 0.002$ (σ) and $^{206}Pb/^{204}Pb = 17.052 \pm 0.003$ (σ).

5. Results

5.1. Fluid inclusions

Five types of FIs were identified on the basis of their phases (liquid–vapor–solid) at room temperature, phase transitions during heating and cooling (−196 to +600 °C) and Laser Raman spectroscopy, including C-type FI ($L + G_{CO2} + L_{CO2}$), W1-type FI ($L + G_{CO2+H2O}$), W2-type FI ($L + G_{H2O}$), S1-type FI ($L + G_{CO2+H2O} + S$) and S2-type FI ($L + G_{H2O} + S$) (Fig. 6).

C-type FIs appear as three phases at room temperature—liquid CO_2, vapor CO_2 and liquid (Fig. 6A, B). They are irregular in shape with sizes of 10–30 μm. W1-type FIs appear as two phases: vapor and liquid (Fig. 6C). The vapor contains $H_2O + CO_2$ and forms CO_2-clathrate under low temperatures. W2-type FIs consist of two phases: liquid H_2O and vapor H_2O (Fig. 6E, F, G). S1-type FIs consist of three phases: liquid, vapor and solid (Fig. 6H); the vapor constitutes of $H_2O + CO_2$. S2-type FIs appear as three phases: liquid, vapor and solid (Fig. 6I).

Numerous FIs in garnet, quartz, sphalerite and calcite from two blocks are suitable for analysis, whereas the FIs in calcite from the Jinla block are too small (Fig. 8). S1- and S2-type FIs are widespread in garnet but rare in quartz and sphalerite. Most daughter minerals in S-type FIs are halite, the other are calcite. A few C-type FIs occur in quartz; only two are suitable for analysis. The quartz from the Jinla block contains W1- and W2-types FIs, whereas the Mangha block mainly consists of W2-type FIs. Boiling FIs occur in quartz of the V1 orebody (Fig. 6D). Laser Raman data show that the content of CO_2 decreases from quartz-sulfide veins to calcite-sulfide veins.

The fluid inclusion microthermometric results of the Cangyuan deposit are shown in Table 1 and Figs. 7–9. The total homogenization temperatures of S-type FIs from garnet range from 462 °C to 498 °C, with salinities of 54.5–58.4 wt% NaCl equivalent. The melting temperatures of the solid CO_2 ($T_{m,\ CO2}$) of C-type FIs range from −59.0 to −56.6 °C, which is slightly below the triple point of pure CO_2 (−56.6 °C). This indicates that the vapor consists of CO_2. Two C-type FI in quartz yield $T_{m,\ cla}$ of 9.1 °C, corresponding to low salinity of 1.8 wt% NaCl equivalent. In the Jinla block, the melting temperatures of clathrates ($T_{m,\ cla}$) are between 4.9 °C and 9.5 °C, whereas the ice ($T_{m,\ ice}$) melting temperatures are between −1.2 °C and −6.2 °C, corresponding to salinities of 1.1–9.5 wt% NaCl equivalent. The homogenization temperatures range from 267 °C to 397 °C. In the Mangha block, fluid inclusions from the quartz-sulfide stage yield $T_{m,\ ice}$ values of −4.1 °C to −0.7 °C, salinities of 1.2–6.6 wt% NaCl equivalent and homogenization temperatures of 260 °C to 340 °C. The fluid inclusions from the calcite-sulfide stage show $T_{m,\ ice}$ values of −4.1 °C to −1.3 °C, salinities of 2.4–6.6 wt% NaCl equivalent, and homogenization temperatures of 280 °C to 329 °C.

Some S-type FIs from garnet are totally homogenized via vapor disappearance, indicating that these FIs are entrapments of an oversaturated solution resulted from transient boiling and volatile escape. The coexistence of different type FIs with similar homogenization temperatures in a microdomain (as exemplified in Fig. 6D) strongly suggests that the fluid boiled at least in the quartz from the V1 orebody. The existence of immiscible fluid inclusion assemblage in garnet or quartz permits reliable estimation of pressure

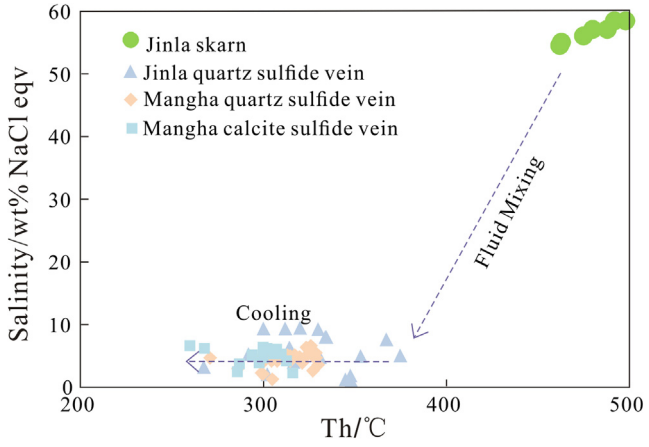

Fig. 7. Salinity vs. Homogenization temperature diagram for FIs from the Cangyuan ore deposit.

Table 1
Microthermometric data of fluid inclusions in different stages from the Cangyuan deposit.

	Stage	Host mineral	FI type	Number	Tm_{clath} (°C)	Tm_{ic} (°C)	Th_{tot} (°C)	Salinity (wt% Nacl)	Estimated trapping pressure (bar)
Jinla	Skarn	Garnet	S2	7			462–498	54.5–58.4	380–420
	Quartz sulfide	Quartz	W2	33		−1.2 to −6.2	267–397	2.1–9.5	74–166
			W1	7	4.9–9.5		330–374	1.1–9.2	154–159
			S1	1		−5.1	335	8	130
Mangha	Quartz sulfide	Quartz	W2	41		−0.7 to −3.9	271–340	1.2–6.2	54–126
			C	2	9.1		290	1.8	73
		Sphalerite	W2	20		−1.3 to −4.1	260–317	2.4–6.6	44–105
	Calcite sulfide	Calcite	W2	9		−3 to −4.1	323–329	5.0–6.6	113–123
		Sphalerite	W2	2		−1.3 to −4.1	286	2.4–3.7	68–70

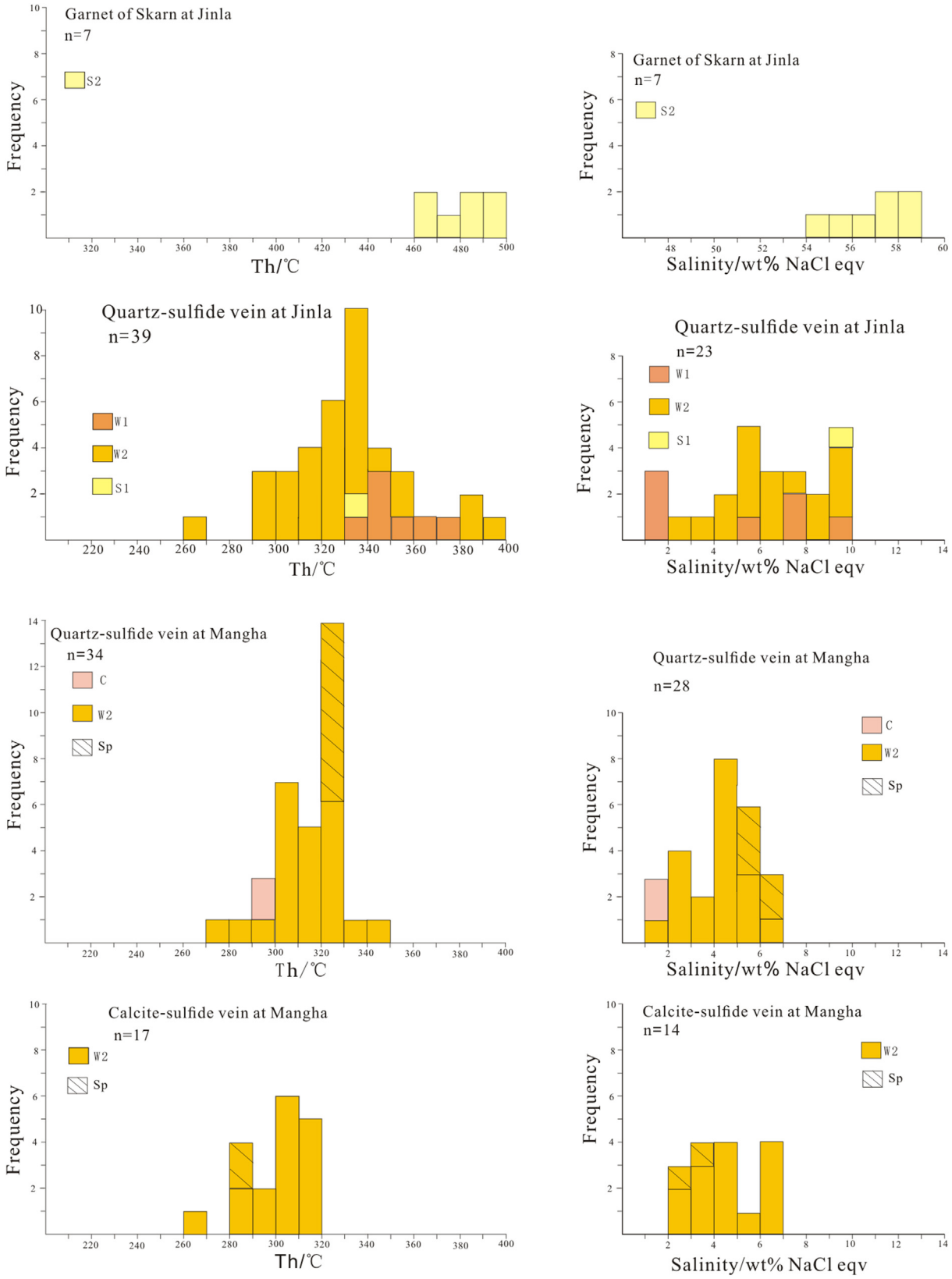

Fig. 8. Salinity and temperature for FIs from the Cangyuan ore deposit.

conditions of fluid trapping during ore formation (Roedder and Bodnar, 1980).

The estimated trapping pressures of the skarn stage, the quartz–sulfide stage in the Jinla and Mangha ore blocks are 380–420 bar, 74–166 bar and 45–126 bar, respectively, that at the calcite-sulfide stage is 68–123 bar. The trapping pressures of the skarn stage cluster around 400 bar, corresponding to a lithostatic depth of 1.5 km, given 2.7 g/cm^3 as the density of upper crust rocks.

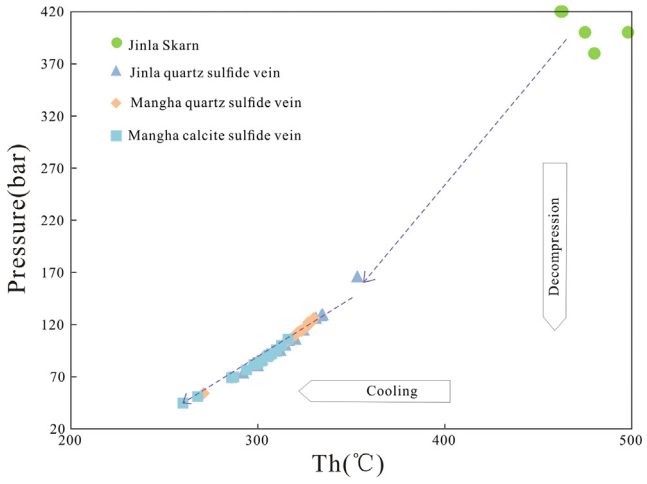

Fig. 9. Minimum trapping pressure vs. homogenization temperature of the Cangyuan deposit.

The average trapping pressure of the quartz sulfide stage is 109 bar. As the quartz-sulfide veins infilled former fractures, the trapping pressure of the quartz sulfide stage corresponds to a hydrostatic depth of 1.1 km. Thus, the Cangyuan deposit was formed at depth of 1.1–1.5 km.

Table 2
$\delta^{18}O$, δD values (‰) of the Cangyuan, Hetaoping, Laochang and Jinman deposits.

Mineral	Temperature (°C)	δD_{H2O}	$\delta^{18}O_{H2O}$
Canyuan	380	−120	3.7
Quartz			
Quartz	370	−108	4.8
Quartz	370	−93	2.6
Quartz	370	−93	3.9
Quartz	327	−106	3.5
Quartz	340	−82	2.9
Quartz	312	−120	3.8
Quartz	299	−105	4.8
Quartz	358	−103	7.7
Quartz	277	−108	6.8
Quartz	329	−107	7.7
Quartz	253	−111	6.8
Quartz	274	−117	7
Quartz	286	−116	8.8
Hetaoping			
Quartz		−105	6.5
Quartz		−100	6.6
Quartz		−102	7.6
Quartz		−108	7.5
Laochang			
Quartz	276	−92	9.2
Quartz	276		9.4
Quartz	264	−93	4.1
Quartz	259	−67.2	−5.4
Quartz	246	−48.2	−7.9
Quartz	308	−46.2	−7.2
Quartz	252	−62.2	−9.5
Jinmang			
Quartz		−51	5.4
Quartz		−101	7.3
Quartz		−86	5.2
Quartz		−102	4.4

Notes: The temperatures used in calculation are the peak values of fluid inclusion homogenization temperatures for individual samples or mineralization stages. The $\delta^{18}O_{H2O}$ of ore fluids in equilibrium with quartz is calculated using equations of $1000\ln\alpha_{quartz\text{-}water} = 3.38 \times 10^6 T^{-2} - 3.40$ (Clayton et al., 1972). Some data is after Yang (2010), Hetaoping is after Xue et al. (2008), Laochang is after Zhao et al. (2012) and Jinman is after Ji and Li (1998).

5.2. H-O isotopes

The analytical data on the oxygen and hydrogen isotopes of quartz and the calculated $\delta^{18}O_{H2O}$ values of the ore forming fluids are listed in Table 2. The $\delta^{18}O$ and δD values of the ore forming fluids range from 2.6‰ to 7.7‰ and from −82‰ to −120‰. The results overlap with the data of previous research ($\delta^{18}O_{H2O}$: 3.8–8.8‰; δD: −105 to −120‰; Yang, 2010). The data of the Hetaoping (Xue et al., 2008), Jinman (Ji and Li, 1998) and Laochang deposits (Zhao et al., 2012) show similar trends with those of the Cangyuan deposit (Fig. 10). The Hetaoping deposits is a skarn type deposit, located to the north of the Cangyuan deposit, with an ore forming age of 116.1 ± 3.9 Ma (Tao et al., 2010); The Laochang deposit is related to granites, which yield a zircon U-Pb age of 43.78 ± 0.78 Ma (Zhao et al., 2012). It is situated in the Changning-Menglian Suture; The Jinman deposit is a vein type Cu deposit, hosted in the west of Lanping Basin and controlled by the NS-trending faults. The faults formed in Tertiary and acted as tunnels for mineralization (Xu et al., 2003).

5.3. Sulfur isotopes

The sulfur isotopic compositions of the Cangyuan deposit are summarized in Table 3 and Fig. 11. The results show a narrow range from −2.3 to 3.2‰. The sulfur isotopic compositions of the Jinla ore block range from −1.5 to 3.1‰, whereas those of the Mangha ore block range from −2.3 to 3.2‰. The pyrite, sphalerite and galena from the Jinla block show relative order of $\delta^{34}S$ enrichment: $\delta^{34}S_{py} > \delta^{34}S_{sp} > \delta^{34}S_{gn}$. The sphalerite, pyrrhotite and galena from the Mangha block show $\delta^{34}S_{sp} > \delta^{34}S_{po} > \delta^{34}S_{gn}$. In addition, the sulfur isotopic compositions of the sulfides have linear correlation (Fig. 12). The sulfur isotopic compositions of the Cangyuan deposit are similar to those of the Lanuoma, Laochang and Jinman deposits (Fig. 11). The three deposits are located to the east of Baoshan Block, close to the Cangyuan deposit. However, the sulfur isotopic compositions of the Cangyuan deposit are distinguished from those of the Jinding deposit (−42.1 to −7.7‰; Tang, et al., 2014).

5.4. Pb isotopes

Lead isotopic compositions of sulfide, K-feldspar and porphyry from the Cangyuan, Laochang, Jinding and Jinman deposits are

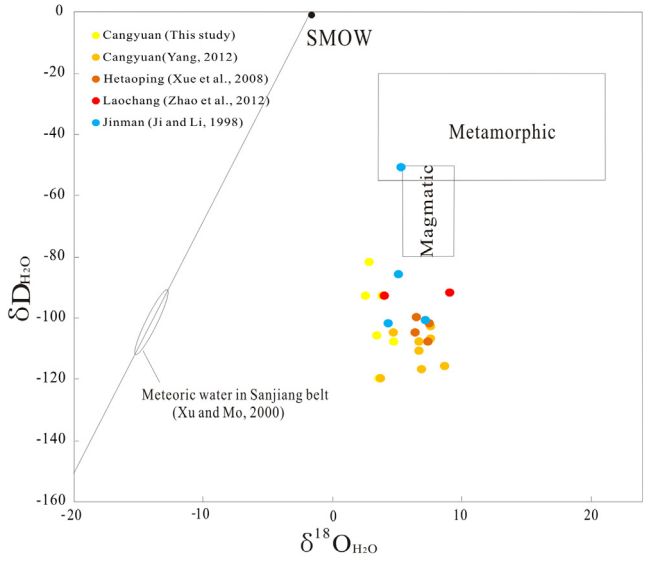

Fig. 10. H, O isotope geochemistry for mineralization fluids of the Cangyuan deposit, data for the Hetaoping, Laochang and Jinman deposits are from Xue et al. (2008), Zhao et al. (2012) and Ji and Li (1998).

Table 3
Sulfur isotopic data for the Cangyuan, Lanuoma, Laochang and Jinman deposits.

Mineral	$\delta^{34}S$(CDT)‰	Mineral	$\delta^{34}S$(CDT)‰
Jinla block		Mangha block	
Gn	0.133	Py	−0.338
Sp	2.217	Sp	0.571
Py	3.072	Gn	−0.928
Gn	−0.179	Po	0.169
Gn	−0.126	Sp	0.458
Py	2.132	Po	−0.565
Py	2.325	Gn	−1.483
Sp	2.084	Gn	−1.496
Py	2.682	Py	−0.394
Sp	1.888	Po	1.320
Gn	0.578	Sp	2.146
Gn	−0.982	Sp	3.173
Py	1.101	Gn	−0.670
Sp	1.685	Sp	1.280
Gn	−1.499	Gn	−0.413
Py	2.143	Gn	−0.546
Py	2.061	Sp	−0.649
Gn	−0.226	Gn	−2.291
Sp	0.733		
Mineral	$\delta^{34}S$(CDT)‰	Mineral	$\delta^{34}S$(CDT)‰
Laochang, after Zhao et al. (2012)		Lanuoma, after Tao et al. (2011)	
py	1.800	Ro	1.400
py	−1.100	Ro	2.400
Gn	−2.400	Ro	0.100
Sp	−3.300	Ro	0.200
Sp	−1.100	Ro	−0.400
Mo	−1.020	Ro	2.300
Mo	−1.050	Ro	0.200
Mo	−3.990	Sp	−0.300
Mo	0.300	Sp	2.600
porphyry	10.060	Sp	0.800
porphyry	3.560	Sp	−1.600
porphyry	3.000		
porphyry	3.340		
porphyry	7.150		
Mineral	$\delta^{34}S$(CDT)‰	Mineral	$\delta^{34}S$(CDT)‰
Jinman, after Ji and Li (1998)		Jinman, after Ji and Li (1998)	
Ter	−4.200	Sp	−0.268
Ccp	−3.432	Sp	−0.542
Bn	−3.400	Sp	−0.693
Bn	−2.620	Sp	−0.350
Bn	−2.325	Ccp	0.159
Ter	−1.382	Bn	1.481
Ccp	−1.573	Ter	2.687
Ter	−1.492	Py	4.196
Ccp	−1.389		

Abbreviation: Mo, molybdenite; Ter, terahedrite; Bn, bornite; Ro, robinsonite; Py, pyrite; Gn, galena; Sp, sphalerite; Ccp, chalcopyrite; Po, pyrrhotite.

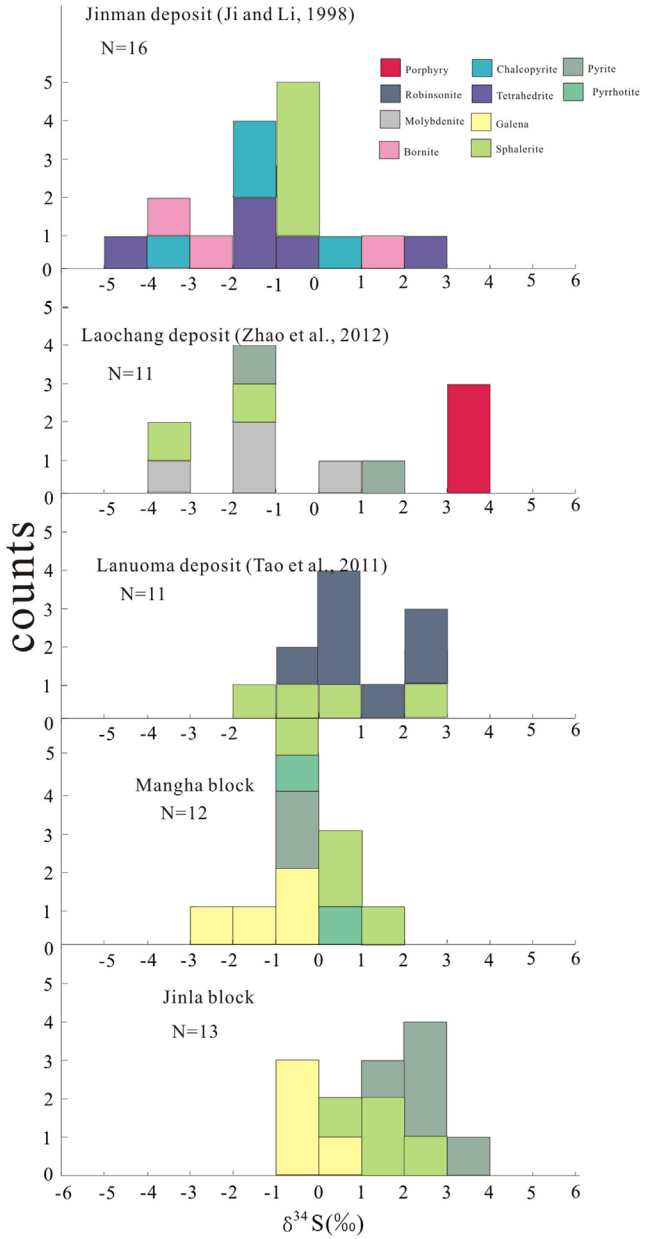

Fig. 11. Histograms of S isotope for sulfides, data for the Lanuoma, Laochang and Jinman deposits are from Tao et al. (2011), Zhao et al. (2012) and Ji and Li (1998).

summarized in Table 4 and Fig. 13. Sulfides from the Jinla ore block have $^{206}Pb/^{204}Pb$, $^{207}Pb/^{204}Pb$ and $^{208}Pb/^{204}Pb$ values of 18.538–18.648, 15.600–15.723 and 38.783–39.149 with averages of 18.637, 15.686 and 38.971, respectively. Sulfides from the Mangha ore block yield $^{206}Pb/^{204}Pb$, $^{207}Pb/^{204}Pb$ and $^{208}Pb/^{204}Pb$ values of 18.680–18.745, 15.706–15.742 and 39.042–39.166 with averages of 18.704, 15.723 and 39.089, respectively. The K-feldspars of granitic rocks in the deposit have $^{206}Pb/^{204}Pb$, $^{207}Pb/^{204}Pb$ and $^{208}Pb/^{204}Pb$ values of 18.603–18.803, 15.620–15.802 and 38.776–39.263, with averages of 18.680, 15.684 and 38.963, respectively.

6. Discussion

6.1. Origin of the ore-forming fluids and materials

The hydrogen–oxygen isotopic compositions of ore-forming fluids from the Cangyuan deposit plot beneath the field of magmatic water (Fig. 10), which is similar to that of the Hetaoping Pb-Zn deposit, Jinman Cu deposit and Laochang Cu-Pb-Zn deposit. The three deposits are located in the west of the Lanping Basin. Former studies suggest the ore-forming fluids of the three deposits are derived from magmatic water mixed with meteoric water (Xue et al., 2008; Zhao et al., 2012; Ji and Li, 1998). Thus, we propose that the ore forming fluids of the Cangyuan deposit are derived from magmatic fluids mixed with meteoric water. Besides, magmatic fluids should be effective in the formation of these Cenozoic deposits located in the west of Lanping Basin.

The homogenization temperatures of the Cangyuan deposit are higher than temperatures for bacterial sulfate reduction (BSR) and thermochemical sulfate reduction (TSR) (Hoefs, 2004; Machel et al., 1995; Ohmoto, 1972); the sulfur isotopic compositions of the sulfides show linear correlation (Fig. 12), indicating these sulfides are in thermodynamics equilibrium and sulfur isotopic fractionation was minimal. Hence, the sulfur in the ore forming fluids should exist as HS^- or S^{2-} other than SO_4^{2-} during transportation. The sulfide ores of the Cangyuan deposit are dominated by

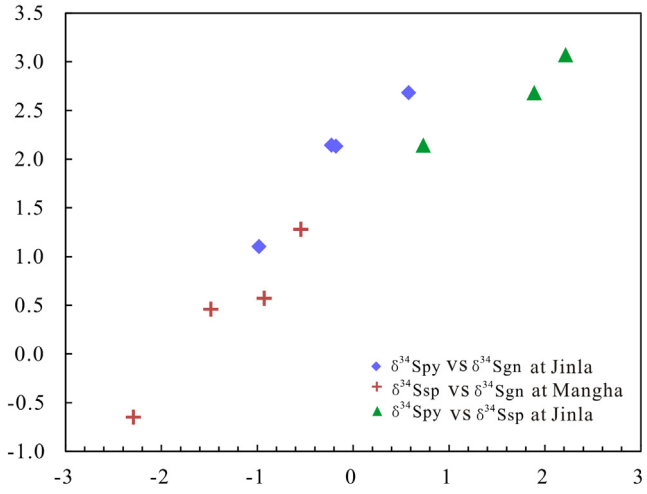

Fig. 12. Sulfur isotope Harker diagram of the Cangyuan deposit, there are linear relationships between δ^{34}Spy and δ^{34}Ssp, δ^{34}Spy and δ^{34}Sgn at the Jinla block, δ^{34}Spy and δ^{34}Sgn at the Mangha block. Abbreviation: Py, pyrite; Sp, sphalerite; Gn, galena.

pyrrhotite, sphalerite, galena, and pyrite. Consequently, the δ^{34}S values of sulfides reflect that of the ore forming fluids (Ohmoto, 1972).

Sulfur isotopic compositions of the Cangyuan deposit (−2.3 to 3.2‰) resemble those of Laochang skarn Cu-Pb-Zn deposit (−4.0 to 7.2‰), Jinman Cu deposit (−4.2 to 4.2‰) and Lanuoma Pb-Zn deposit (−1.6 to 2.6‰). The Sulfur of the three deposits is thought to be derived from the magma (Zhao et al., 2012; Ji and Li, 1998; Tao et al., 2011; Ding et al., 2016), which suggests that the sulfur of the Cangyuan deposit is derived dominantly from magma. However, sulfur isotopic data of the Jinding deposit show highly variable δ^{34}S values (−42.1 to −7.7‰) of different ore types, indicating multiple sulfur sources (biogenic sulfur + evaporites) and formation mechanisms for reduced sulfur (Tang, et al., 2014). This may be due to the fact that the Cangyuan, Laochang, Jinman and Lanuoma deposits are situated to the west of the Lanping-Changdu Basin, with Cenozoic granites close to the deposits, whereas the Jinding deposit developed in the continental basin. Thus, we propose that magmatic sulfur is involved in the formation of deposits located in the west of Mesozoic continental basin.

As shown in Fig. 13, the lead isotopic compositions of sulfides from the Cangyuan deposit show linear correlations in $^{206}Pb/^{204}Pb$,

Table 4
Lead isotope data of the Cangyuan, Laochang, Jinding and Jinman deposits.

Mineral	$^{208}Pb/^{204}Pb$	$^{207}Pb/^{204}Pb$	$^{206}Pb/^{204}Pb$	Mineral	$^{208}Pb/^{204}Pb$	$^{207}Pb/^{204}Pb$	$^{206}Pb/^{204}Pb$
The Cangyuan deposit				Upper Mantle after Zhang et al. (2002)			
Sp	38.931	15.723	18.602	Basalt	37.797	15.456	17.877
Py	39.065	15.692	18.633	Basalt	37.797	15.523	18.353
Py	39.070	15.699	18.641	Basalt	38.414	15.523	17.877
Py	38.783	15.600	18.538	Basalt	38.414	15.456	18.353
Py	39.149	15.722	18.675	Laochang, after Zhao et al. (2012)			
Gn	38.944	15.683	18.647	Py	38.950	15.686	18.657
Gn	38.949	15.684	18.647	Py	39.053	15.716	18.688
Gn	38.957	15.686	18.645	Py	37.753	15.452	17.874
Gn	38.964	15.689	18.646	Py	37.771	15.448	17.863
Gn	38.950	15.684	18.645	Gn	39.007	15.703	18.677
Gn	38.965	15.688	18.648	Sp	39.104	15.733	18.701
Gn	38.969	15.688	18.647	Sp	38.646	15.656	18.505
Gn	38.965	15.687	18.646	Porphyry	38.695	15.614	18.561
Gn	38.953	15.684	18.645	Porphyry	38.246	15.652	17.988
Gn	38.967	15.688	18.647	Porphyry	38.766	15.661	18.552
Gn	38.946	15.682	18.643	Porphyry	38.405	15.586	18.205
Gn	39.064	15.711	18.684	Porphyry	38.623	15.601	18.426
Gn	39.049	15.707	18.680	Porphyry	38.774	15.620	18.564
Gn	39.048	15.706	18.680	Porphyry	38.910	15.663	18.621
Gn	39.166	15.742	18.745	Porphyry	38.524	15.628	18.283
Gn	39.097	15.723	18.706	Jinding, after Zhang et al. (1993)			
Gn	39.114	15.729	18.711	Gn	38.463	15.612	18.400
Gn	39.109	15.727	18.710	Gn	38.660	15.632	18.441
Gn	39.112	15.727	18.712	Gn	38.300	15.491	18.285
Po	39.042	15.731	18.712	Gn	38.290	15.501	18.303
K-feldspar of granitic rocks for the deposit				Gn	38.536	15.628	18.420
K-pl	38.776	15.620	18.604	Gn	38.174	15.476	18.232
K-pl	39.263	15.802	18.803	Gn	38.295	15.493	18.283
K-pl	38.814	15.631	18.697	Gn	38.235	15.450	18.321
K-pl	38.905	15.653	18.723	Gn	38.557	15.640	18.506
K-pl	38.879	15.630	18.722	Gn	38.488	15.619	18.493
K-pl	38.812	15.631	18.688	Gn	38.090	15.430	18.220
K-pl	38.942	15.678	18.659	Gn	38.010	15.380	18.210
K-pl	38.982	15.673	18.669	Gn	38.050	15.400	18.210
K-pl	39.118	15.727	18.722	Gn	38.040	15.360	18.170
K-pl	39.058	15.715	18.705	Gn	38.230	15.410	18.270
K-pl	38.983	15.650	18.770	Gn	38.300	15.420	18.290
K-pl	39.093	15.735	18.723	Gn	38.160	15.410	18.220
K-pl	39.014	15.707	18.687	Jinman, after Xu and Zhou (2004)			
K-pl	39.005	15.721	18.668	Ter	38.555	15.590	18.559
K-pl	38.922	15.681	18.654	Ter	38.605	15.581	18.628
K-pl	39.034	15.721	18.711	Ter	38.615	15.586	18.639
K-pl	38.877	15.670	18.635				
K-pl	38.866	15.661	18.650				
K-pl	38.972	15.680	18.665				

Table 4 (*continued*)

Mineral	$^{208}Pb/^{204}Pb$	$^{207}Pb/^{204}Pb$	$^{206}Pb/^{204}Pb$	Mineral	$^{208}Pb/^{204}Pb$	$^{207}Pb/^{204}Pb$	$^{206}Pb/^{204}Pb$
K-pl	38.916	15.675	18.657				
K-pl	38.981	15.692	18.661				
K-pl	38.900	15.665	18.625				
K-pl	39.020	15.701	18.662				
K-pl	38.920	15.667	18.662				
K-pl	38.880	15.656	18.603				
K-pl	39.072	15.725	18.689				
K-pl	38.986	15.698	18.652				

Abbreviation: Ter, terahedrite; Py, pyrite; Gn, galena; Sp, sphalerite; K-pl, K-feldspar.

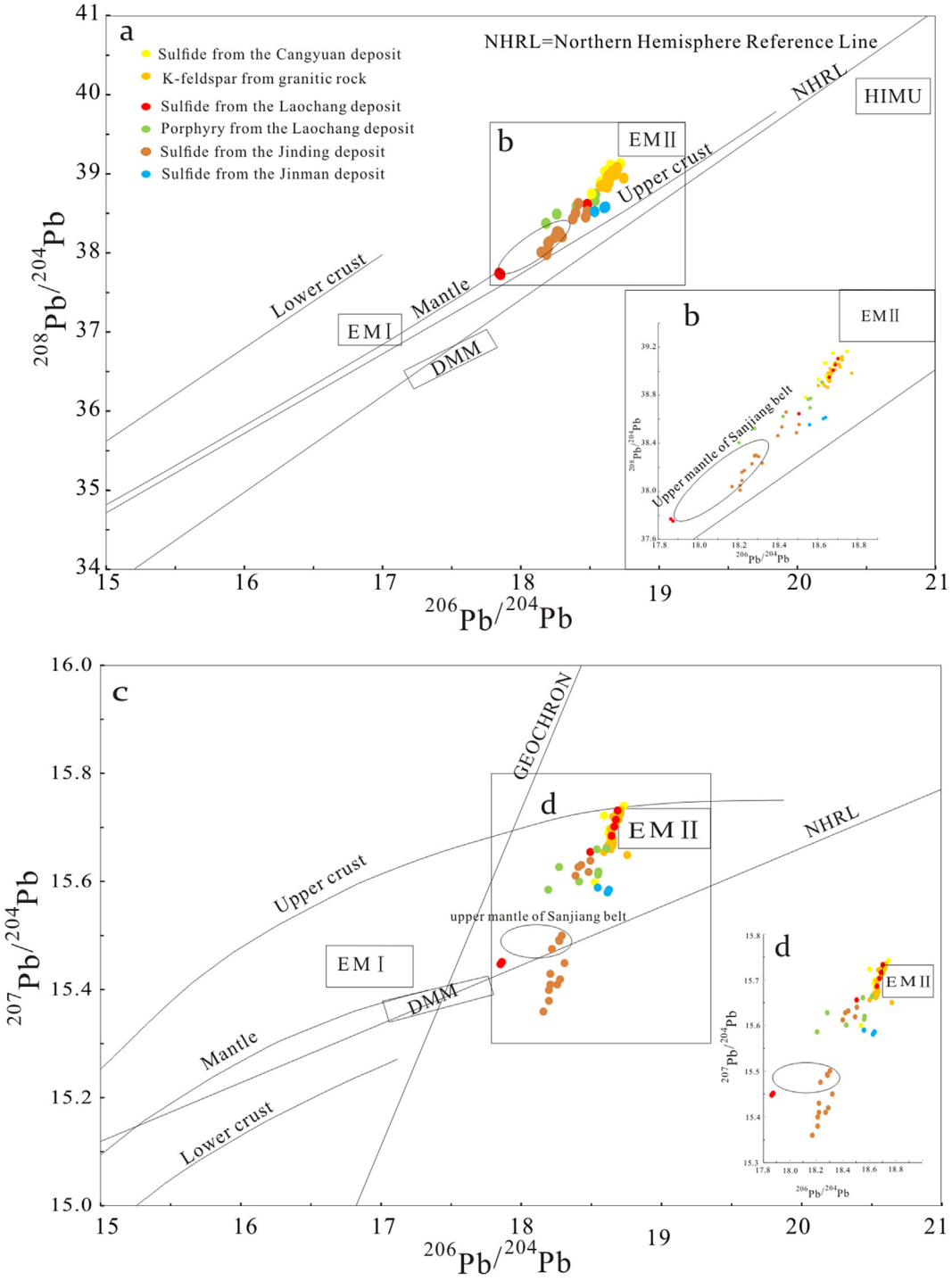

Fig. 13. Lead isotope plots of sulfides and related granitic rock K-feldspars from the Cangyuan deposit. Reference lines are based on Zartman and Doe (1981), data for the Laochang, Jinding and Jinman deposits are from Zhao et al. (2012), Zhang et al. (1993) and Xu and Zhou. (2004).

$^{207}Pb/^{204}Pb$ and $^{208}Pb/^{204}Pb$. The lead isotopic compositions of K-feldspar from granitic rocks overlap with those of sulfides in the deposit, indicating that the ores and the granitic rocks share a same metal source. The lead isotopic compositions of ore sulfides and K-feldspars from the granitic rocks are distributed in a domain between the mantle, upper crust and EMII, which supports the idea that the porphyry is syntectic type as Yang (2010) suggested. The lead isotopic compositions of the Cangyuan deposit are similar to those of Laochang granite porphyry, which is formed by mixing of the mantle and crust (Yang et al., 2012). Besides, they share same linear relationship but different values with those of Jinding and Jinman deposits. Compared with the Jinding deposit, the data of the Jinman deposit plot closer the Cangyuan deposit. The ore metals of the latter two deposits are suggested to be derived from the basin with mantle injection (Tang et al., 2014). Thus, the metals of the Cangyuan deposit should be derived from a multiple source (upper mantle and crust). As seen in Fig. 13, the lead isotopic compositions of the four deposits are increasing from the Jinding deposit in the east to the Cangyuan deposit in the west. This may be related to the geology setting. Lead from the crust should contribute more to the mineralization in the Jinding deposit than the Cangyuan deposit.

In view of H-O, S and Pb isotopes, the deposits in the west of Lanping-Changdu Basin including Laochang, Lanuoma and Jinman share many similarities with the Cangyuan deposit. Magmatic fluids contribute to the formation of these deposits, whereas the Jinding deposit are distinguished from the Cangyuan deposit in isotope geochemical characters. The Jinding deposit are formed due to basin brine though its inert gas and lead isotopic compositions go against with the conclusion (Xue et al., 2007; Zhang et al., 1993; Tang et al., 2014).

6.2. Characteristics and evolution of ore-forming fluids

The microthermometry data of the fluid inclusions are shown in Table 1. The initial ore forming fluids of the Cangyuan deposit were high temperatures (462–498 °C) and high salinities (54.5–58.4 wt% NaCl equivalent) during the skarn stage; afterward, the fluids evolved to mesothermal (260–397 °C) and low salinity (1.2–9.5wt% NaCl equivalent) during the sulfide stage (Fig. 7). The homogenization temperatures of fluid inclusions decreased through the sulfide stage with constant salinities: Quartz in the Jinla block (267–397 °C); Quartz/sphalerite in the Mangha block (260–340 °C); Calcite-sulfide veins in the Mangha ore block (286–329 °C).

As shown in Fig. 7, the salinities decreased with temperatures drop during the skarn stage but remained constant as temperatures decreased during the sulfide stage. This indicates fluid mixing contributes to metals precipitation adjacent to the skarn stage, whereas cooling contributes to mineralization during the sulfide stage. Fig. 9 shows a tremendous decrease in pressure between the skarn stage and the sulfide stage, which implies that decompression plays an important role in metal precipitation during the skarn stage.

6.3. Possible mechanism of metals transport and deposition

Experimental research has shown that sulfide complexes and chloride complexes of Pb^{2+}, Zn^{2+} and Ag^{+} play important roles in the transportation of metals in hydrothermal solutions (Seward, 1976; Ruaya and Seward, 1986; Seward and Barnes, 1997). As previously mentioned, the sulfur from the Cangyuan deposit exists as HS^{-} or S^{2-} in hydrothermal fluids. The mineral assemblage of calcite + pyrite + pyrrhotite in the Mangha block indicates ore-forming fluids of low f_{O2} and high pH (Ohmoto and Rye, 1979). Cole and Drummond (1986) demonstrated that sulfide complexes are unstable under high pH. Consequently, sulfide complexes are unstable during transportation in the ore-forming fluids of the Cangyuan deposit. Our study shows the daughter minerals of S-type FIs from garnet are mainly halite, which suggests that the initial ore-forming fluids are NaCl-H_2O. That is, chloride complexes play important roles in the transportation of metals in hydrothermal solutions.

Hydrothermal deposits are formed by the instability of metal complexes (Seward and Barnes, 1997). Boiling (Calagari, 2004), fluid mixing (O'Neil and Silberman, 1974), cooling (Landtwing et al., 2005) and fluid-rock interaction (Beane and Titley, 1981) can play important roles in the deposition of sulfides from ore-forming fluids.

The boiling process of magmatic fluids results in coexisting vapor–rich and vapor–poor inclusions (Bodnar and Vityk, 1994). Our study shows that boiling inclusions occur in quartz from V1 orebody. This suggests that the boiling process contributes to metal deposition at least in V1 orebody.

Fluid mixing between magmatic fluids and meteoric water could play an important role in the deposition of metals from ore-forming fluids (Beane and Titley, 1981). The fluid-mixing model is required as follows: firstly, the hydrogen–oxygen isotope data are between magmatic water and meteoric water; secondly, the salinities of ore-forming solutions decrease with temperatures (Simmons et al., 2005). The hydrogen and oxygen isotope compositions of the Cangyuan deposit plotted beneath the area of magmatic water and shifted from the meteoric water line (Fig. 10). The salinities of ore-forming fluids decreased rapidly from the skarn stage to the sulfide stage and remained constant during sulfide stage (Fig. 7). Thus, mixing model may interpret the deposition of sulfides adjacent to the skarn stage.

Experimental studies have shown that fluid cooling is particularly effective for precipitation of metals from solutions (Liu and McPhail, 2005; Hezarkhani et al., 1999; Redmond et al., 2004). Ore-forming fluids of the Cangyuan deposit show a decrease in temperature with constant salinity through the sulfide stage (Fig. 7). According to experiment results (Liu and McPhail, 2005), the stability of chloride complexes decreases rapidly when the solutions cool over the temperature range of the Cangyuan deposit. Therefore, cooling should provide the largest contribution to sulfides deposition in the Cangyuan deposit.

7. Conclusions

The ore-forming fluids of the Cangyuan deposit were CO_2-bearing, NaCl-H_2O. The initial fluids were high temperatures of 462–498 °C and high salinities of 54.5–58.4 wt% NaCl equivalent during the skarn stage. Afterward, the fluids evolved to mesothermal temperatures of 260–397 °C and low salinities of 1.2–9.5 wt% NaCl equivalent during the sulfide stage. Metals were transported as chloride complexes rather than sulfide complexes in the hydrothermal fluids. Fluid mixing, decompression, boiling and cooling, especially cooling, contributed to the metal precipitation. The hydrogen–oxygen isotopic compositions show that the ore-forming fluids were derived from magma mixed with meteoric water. The sulfur isotopic compositions indicate a magmatic source for the sulfur. The lead isotopic compositions demonstrate that metals of the ore deposit were derived from Cenozoic granite, which is syntectic type derived from mixture of the mantle and crust.

Acknowledgements

The authors appreciate the assistance of Chaojian Qing, Jiali Cai and Ning An for Laser Raman, FIs Micro-thermometric and sulfur

isotope measurements at the Institute of Geochemistry, Chinese Academy of Science. In addition, the authors thank Zhi'an Bao at Northwest University for assisting with in situ lead isotope measurement. This study is supported by the National Basic Research Program of China (2015CB452603) and CAS-SAFEA International Partnership Program for Creative Research Teams (KZZD-EW-TZ-20).

References

Beane, R., Titley, S., 1981. Porphyry copper deposits. Part II: Hydrothermal alteration and mineralization. Economic Geology 75th Anniversary Volume, pp. 235–269.

Bodnar, R.J., 1993. Revised equation and table for determining the freezing point depression of H_2O-NaCl solutions. Geochim. Cosmochim. Acta 57, 683–684.

Bodnar, R.J., Vityk, M.O., 1994. Interpretation of microthermometric data for H2O-NaCl fluid inclusions. Fluid Inclusions Miner.: Methods Appl., 117–130

Brown, P.E., 1989. Flincor: a microcomputer program for the reduction and investigation of fluid-inclusion data. Am. Mineral. 74, 1390–1393.

Brown, P.E., Lamb, W.M., 1989. P-V-T properties of fluids in the system H_2O±CO_2±NaCl: New graphical presentations and implications for fluid inclusion studies. Geochim. Cosmochim. Acta 53, 1209–1221.

Calagari, A.A., 2004. Fluid inclusion studies in quartz veinlets in the porphyry copper deposit at Sungun, East-Azarbaidjan, Iran. J. Asian Earth Sci. 23, 179–189.

Chen, Y.Q., Huang, J.N., Lu, Y.X., 2008. Geochemistry of elements, sulfur-lead isotopes and fluid inclusions from Jinla Pb-Zn-Ag Polymetallic ore field at the joint area across China and Myanmar Border. Earth Sci. 34 (4), 585–594.

Chen, H., Li, F., Jian, R.T., Luo, S.L., Yao, W., 2010. Zircon SHRIMP dating of the Laochang granite porphyry in Lancang, Yunnan and its geological significance. Acta Geol. Sinica 84, 485–491 (in Chinese with English abstract).

Chen, X.C., Hu, R.Z., Bi, X.W., Li, H.M., Lan, J.B., Zhao, C.H., Zhu, J.J., 2014. Cassiterite LA-MCICP-MS U/Pb and muscovite $^{40}Ar/^{39}Ar$ dating of tin deposits in the Tengchong Lianghe tin district, NW Yunnan, China. Miner. Deposita 49, 843–860.

Chung, S.L., Lo, C.H., Lee, T.Y., Zhang, Y.Q., Xie, Y.W., Li, X.H., Wang, K.L., Wang, P.L., 1998. Diachronous uplift of the Tibetan plateau starting 40 Myr ago. Nature 394, 769–773.

Clayton, R.N., O'Neil, J.R., Mayeda, T.K., 1972. Oxygen isotope exchange between quartz and water. J. Geophys. Res. 77, 3057–3067.

Cole, D.R., Drummond, S.E., 1986. The effect of transport and boiling on Ag/Au ratios in hydrothermal solutions: a preliminary assessment and possible implications for the formation of epithermal precious-metal ore deposits. J. Geochem. Explor. 1986 (25), 45–79.

Collins, P.L.F., 1979. Gas hydrates in CO_2-bearing fluid inclusions and the use of freezing data for estimation of salinity. Econ. Geol. 74, 1435–1444.

Deng, J., Wang, Q.F., Li, G.J., Li, C.S., Wang, C.M., 2013. Tethys tectonic evolution and its bearing on the distribution of important mineral deposits in the Sanjiang region, SW China. Gondwana Res. 26, 419–437.

Deng, J., Wang, Q., Li, G., Santosh, M., 2014. Cenozoic tectono-magmatic and metallogenic processes in the Sanjiang region, southwestern China. Earth Sci. Rev. 138, 268–299.

Ding, T., Ma, D., Lu, J., Zhang, R., Zhang, S., 2016. S, Pb, and Sr isotope geochemistry and genesis of Pb-Zn mineralization in the Huangshaping polymetallic ore deposit of southern Hunan Province, China. Ore Geol. Rev. 77, 117–132.

Dupont-Nivet, G., Lippert, P.C., van Hinsbergen, D.J., Meijers, M.J., Kapp, P., 2010. Palaeolatitude and age of the Indo-Asia collision: palaeomagnetic constraints. Geophys. J. Int. 182, 1189–1198.

Guo, L.G., Liu, Y.P., Xu, W., Zhang, X.C., Qin, K.Z., Li, T.S., Shi, Y.R., 2006. Constraints to the mineralization age of the Yulong porphyry copper deposit from SHRIMP U-Pb zircon data in Tibet. Acta Petrol. Sin. 22 (4), 1009–1016 (in Chinese with English abstract).

Hall, D.L., Sterner, S.M., Bodnar, R.J., 1988. Freezing point depression of NaCl-KCl-H_2O solutions. Econ. Geol. 83, 197–202.

Hezarkhani, A., Williams, J.A., Gammons, C., 1999. Factors controlling copper solubility and chalcopyrite deposition in the Sungun porphyry copper deposit. Iran. Miner. Deposita 34, 770–783.

Hoefs, J., 2004. Stable Isotope Geochemistry. Springer-Verlag, Berlin, p. 201.

Hou, Z.Q., Ma, H.W., Zaw, K., Zhang, Y.Q., Wang, M.J., Wang, Z., Pan, G.T., Tang, R.L., 2003. The Himalayan Yulong porphyry copper belt: product of large-scale strike-slip faulting in Eastern Tibet. Econ. Geol. 98, 125–145.

Hou, Z.Q., Zaw, K., Pan, G., Mo, X.X., Xu, Q., Hu, Y.Z., Li, X.Z., 2007. Sanjiang Tethyan metallogenesis in SW China: tectonic setting, metallogenic epochs and deposit types. Ore Geol. Rev. 31, 48–87.

Ji, H.B., Li, C.Y., 1998. Geochemical characteristics and source of ore-forming fluid for Jinman copper deposit in western Yunnan Province, China. Acta Mineralogica Sinica 18, 28–37.

Jiang, Y.H., Jiang, S.Y., Ling, H.F., Dai, B.Z., 2006. Low-degree melting of a metasomatized lithospheric mantle for the origin of Cenozoic Yulong monzogranite-porphyry, east Tibet: geochemical and Sr-Nd-Pb-Hf isotopic constraints. Earth Planet. Sci. Lett. 241, 617–633.

Landtwing, M., Pettke, T., Halter, W., Heinrich, C., Redmond, P., Einaudi, M., Kunze, K., 2005. Copper deposition during quartz dissolution by cooling magmatic-hydrothermal fluids: the Bingham porphyry. Earth Planet. Sci. Lett. 235, 229–243.

Liang, H.Y., Campbell, I.H., Allen, C., Sun, W.D., Liu, C.Q., Yu, H.X., Xie, Y.W., Zhang, Y.Q., 2006. Zircon Ce^{4+}/Ce^{3+} ratios and ages for Yulong ore-bearing porphyries in eastern Tibet. Miner. Deposita 41, 152–159.

Liu, W., McPhail, D.C., 2005. Thermodynamic properties of copper chloride complexes and copper transport in magmatic-hydrothermal solutions. Chem. Geol. 221, 21–39.

Liu, Z.Q., Li, X.Z., Ye, Q.T., Luo, J.N., Shen, G.F., Mo, X.X., Chen, F.Z., Chen, B.W., Yang, Y.Q., Lü, B.X., Chen, J.S., Pan, G.T., Jia, B.J., Hu, Y.Z., Zheng, L.L., 1993. Division of Tectonomagmatic Belts and Distribution of the Ore Deposits in Sanjiang Region. Geological Publishing House, Beijing, pp. 1–243 (In Chinese with English abstract).

Lu, Y.J., Kerrich, R., Cawood, P.A., McCuaig, T.C., Hart, C.J.R., Li, Z.X., Hou, Z.Q., Bagas, L., 2012. Zircon SHRIMP U-Pb geochronology of potassic felsic intrusions in western Yunnan, SW China: constraints on the relationship of magmatism to the Jinsha suture. Gondwana Res. 22, 737–747.

Machel, H.G., Krouse, H.R., Sassen, R., 1995. Products and distinguishing criteria of bacterial and thermochemical sulfate reduction. Appl. Geochem. 10, 373–389.

Ohmoto, H., 1972. Systematics of sulfur and carbon isotopes in hydrothermal ore deposits. Econ. Geol. 67, 551–578.

Ohmoto H., Rye R.O., 1979. Isotopes of sulfur and carbon. In: Geochemistry of Hydrothermal Ore Deposits, pp. 509–567.

O'Neil, J.R., Silberman, M.L., 1974. Stable isotope relations in epithermal Au-Ag deposits. Econ. Geol. 69, 902–909.

Redmond, P.B., Einaudi, M.T., Inan, E.E., et al., 2004. Copper deposition by fluid cooling in intrusion-centered systems: New insights from the Bingham porphyry ore deposit, Utah. Geology 32, 217–220.

Roedder, E., Bodnar, R.J., 1980. Geologic pressure determinations from fluid inclusion studies. Ann. Rev. Earth Planet. Sci. 8, 263–301.

Ruaya, J.R., Seward, T.M., 1986. The stability of chlorozinc (II) complexes in hydrothermal solutions up to 350°C. Geochim. Cosmochim. Acta 50, 651–661.

Rui, Z.Y., Huang, C.K., Qi, G.M., Xu, J., Zhang, M.T., 1984. Porphyry Copper (Molybdenum) Deposits in China. Geological Publishing House, Beijing, pp. 1–350 (In Chinese).

Seward, T., Barnes, H., 1997. Metal transport by hydrothermal ore fluids. In: Barnes, H. (Ed.), Geochemistry of Hydrothermal Ore Deposits. third ed. Wiley, New York, pp. 435–486.

Seward, T.M., 1976. The stability of chloride complexes of Silver in hydrothermal solutions up to 350 °C. Geochim. Cosmochim. Acta 40, 1329–1341.

Simmons, S.F., White, N.C., John, D.A., 2005. Geological characteristics of epithermal precious and base metal deposits. Econ. Geol. 29, 485–522. 100th anniversary.

Song, Y.C., Hou, Z.Q., Yang, T.N., Li, S.J., Wang, F.C., Gao, Y.W., Gong, X.G., Yang, Z.S., Zhang, H.R., Li, L.S., Wang, G.R., Wang, Y.K., Liu, Q., Hao, H.D., 2013. Mineral prospecting and its related approaches in Duocaima Pb-Zn deposit in Tuotuohe, Qinghai Province. Miner. Deposits 32, 744–756 (in Chinese with English abstract).

Tang, R.L., Luo, H.S., 1995. The Geology of Yulong Porphyry Copper (Molybdenum) Ore Belt, Xizang (Tibet). Geological Publishing House, Beijing, pp. 1–320 (In Chinese with English abstract).

Tang, J.X., Zhong, K.H., Liu, Z.C., Li, Z.J., Dong, S.Y., Zhang, L., 2006. Intracontinent orogen and metallogenesis in Himalayan epoch: Changdu large composite basin, eastern Tibet. Acta Geol. Sinica 80, 1364–1376 (in Chinese with English abstract).

Tang, Y.Y., Bi, X.W., Fayek, M., Wu, L.Y., Zou, Z.C., Feng, C.X., Wang, X.S., 2014. Microscale sulfur isotopic compositions of sulfide minerals from the Jinding Zn-Pb deposit, Yunnan Province, southwest China. Gondwana Res. 26, 594–607.

Tao, Y., Zhu, F.L., Ma, Y.S., Ye, L., Chen, Z.T., 2009. LA-LCP-MA zircon U-Pb dating of Zhibenshan granite from Baoshan block. Acta Mineral. Sin. 29, 329 (in Chinese).

Tao, Y., Hu, R.Z., Zhu, F.L., Ma, Y.S., Ye, L., Chen, Z.T., 2010. Ore forming age and the geodynamic background of the Hetaoping lead-zinc deposit in Baoshan, Yunnan. Acta Petrol. Sin. 26, 1760–1772 (in Chinese with English abstract).

Tao, Y., Bi, X., Xin, Z., et al., 2011. Geology, geochemistry and origin of Lanuoma Pb-Zn-Sb deposit in Changdu area, Tibet. Miner. Deposits 30, 599–615.

Williams, H., Turner, S., Kelley, S., Harris, N., 2001. Age of composition of dikes in southern Tibet: new constraints on the timing of east-west extension and its relationship to post collisional magmatism. Geology 29, 339–342.

Xiao, X.N., Yu, X.H., Yang, G.L., Yang, W.G., Mo, X.X., Zeng, P.S., 2008. A study of fluid inclusions from Cangyuan lead-zinc polymetallic ore concentration area in western Yunnan. Miner. Deposits 27 (1), 100–112 (in Chinese with English abstract).

Xu, Q.D., Mo, X.X., 2000. Regional fluid characters and regimes of "Sanjiang" middle belt during Neo-Tethys. Acta Petrol. Sin. 16, 639–648.

Xu, Y.G., Yang, Q.J., Lan, J.B., Luo, Z.Y., Huang, X.L., Shi, Y.R., Xie, L.W., 2012. Temporal-spatial distribution and tectonic implications of the batholiths in the Gaoligong-Tengliang-Yingjiang area, western Yunnan: constraints from zircon U-Pb ages and Hf isotopes. J. Asian Earth Sci. 53, 151–175.

Xu, Y.G., Lan, J.B., Yang, Q.J., Huang, X.L., Qiu, H.N., 2008. Eocene break-off of the NeoTethyan slab as inferred from intraplate-type mafic dykes in the Gaoligong orogenic belt, eastern Tibet. Chem. Geol. 255, 439–453.

Xue, C.J., Wang, D.H., Chen, Y.C., Yang, J.M., 2000. Helium, argon, and xenon isotopic compositions of ore-forming fluids in Jinding-Baiyangping polymetallic deposits, Yunnan, Southwest China. Acta Geol. Sin. 74 (3), 521–528.

Xue, C.J., Chen, Y.C., Yang, J.M., Wang, D.H., Yang, W.G., Yang, Q.B., 2002a. Jinding Pb-Zn deposit: geology and geochemistry. Miner. Deposits 21, 245–281 (in Chinese with English abstract).

Xue, C.J., Chen, Y.C., Yang, J.M., Wang, D.H., 2002b. The CO_2-rich and hydrocarbon-bearing ore-forming fluid and their metallogenic role in the Lanping Pb-Zn-Ag-Cu ore-field, Northwestern Yunnan, China. Acta Geol. Sin. 76 (2), 244–253 (in Chinese with English abstract).
Xue, C.J., Chen, Y.C., Wang, D.H., Yang, J.M., Yang, W.G., 2003. Geology and isotopic composition of helium, neon, xenon and metallogenic age of the Jinding and Baiyangping ore deposits, northwest Yunnan, China. Sci. China, Ser. D Earth Sci. 46 (8), 789–800.
Xue, C.J., Zeng, R., Liu, S.W., Chi, G.X., Qing, H.R., Chen, Y.C., Yang, J.M., Wang, D.H., 2007. Geologic, fluid inclusion and isotopic characteristics of the Jinding Zn-Pb deposit, western Yunnan, South China: a review. Ore Geol. Rev. 31, 337–359.
Xue, C.D., Han, R.S., Yang, H.L., Yang, Z.M., Tian, S.H., Liu, Y.Q., Hao, B.W., 2008. Isotope geochemical evidence for ore-forming fluid resources in Hetaoping Pb-Zn deposit, Baoshan, northwestern Yunnan. Miner. Deposits 27 (2), 243–252 (in Chinese with English abstract).
Yang, G.L., 2010. A study on the Mineralization and Metallogenic Model of Pb-Zn-Ag Polymetallic Ore Concentration in Cangyuan, Yunnan and Jinchang, Myanmar. (A dissertation submitted to China University of Geosciences (Beijing) for doctoral degree), pp. 1–134. (in Chinese with English abstract).
Yang, F., Li, F., Chen, H., 2012. Geochemistry and tectonic setting of the Laochang concealed granite porphyry in Langcang, Yunnan Province. Acta Petrol. Mineral. 31, 39–49 (in Chinese with English abstract).
Zartman, R.E., Doe, B.R., 1981. Plumbotectonics-the model. Tectonophysics 75, 135–162.
Zhang, Q., 1993. Pb isotopic composition of Jinding super-large Pb-Zn in Yunnan Province and discussion on the sources of lead. Geol. Prospect. 29, 21–28 (in Chinese with English abstract).
Zhao, X., Li, F., Yang, F., 2012. Isotopic geochemical evidence of the sources of ore-forming materials for the Laochang deep porphyry Mo (Cu) deposit in Lancang, Yunnan. Acta Petrol. Mineral. 5, 010 (in Chinese with English abstract).
Zhao, X.Y., 1989. Stable isotope geochemistry of the Jinding lead-zinc ore deposit, Yunnan. Earth Sci. 14 (5), 495–501 (in Chinese with English abstract).
Zhou, M.F., Robinson, P.T., Wang, C.Y., Zhao, J.H., Yan, D.P., Gao, J.F., Malpas, J., 2012. Heterogeneous mantle source and magma differentiation of quaternary arc-like volcanic rocks from Tengchong, SE margin of the Tibetan Plateau. Contrib. Miner. Petrol. 163, 841–860.
Zhou, W.Q., Zhou, Q.L., 1992. A study on the isotopic composition of Pb and S in the Lanping Pb-Zn deposit, Yunnan Province. Geochimica 20 (2), 141–148 (in Chinese with English abstract).

Further reading

Qian, Z., Jiayong, P., Jiajun, L., et al., 2002. Determination and application of the upper mantle lead composition in the western Yunnan. Geol. Geochem. 30, 1–6.
Qidong, X., Jianwei, L., 2003. Migration of ore-forming fluids and its relation to zoning of mineralization in northern Lanping Cu-polymetallic metallogenic area, Yunnan Province: evidence from fluid inclusions and stable isotopes. Miner. Deposits 22, 375–384.
Qidong, X., Lian, Z., 2004. Ore-forming fluid migration in relation to mineralization zoning in Cu-polymetallic mineralization district of northern Lanping, Yunnan: evidence from lead isotope and mineral chemistry of ores. Miner. Deposits 4 (004).